*Korean J. Chem. Eng.*, 36(12), 2143-2152 (2019)
DOI: 10.1007/s11814-019-0399-3

pISSN: 0256-1115
eISSN: 1975-7220

# Rapid and reusable detection of hydrogen peroxide using polyurethane scaffold incorporated with cerium oxide nanoparticles

**Pathikrit Saha, Anoth Maharajan, Pritam Kumar Dikshit, and Beom Soo Kim†**

Department of Chemical Engineering, Chungbuk National University, Cheongju, Chungbuk 28644, Korea
(*Received 8 August 2019 • accepted 1 October 2019*)

**Abstract**−We report a novel approach to using a polyurethane scaffold incorporated with cerium oxide nanoparticles as an alternative to the natural enzyme horseradish peroxidase for rapid and reusable detection of hydrogen peroxide. After the preparation of polyurethane from soybean oil and malic acid, cerium or iron oxide nanoparticles were synthesized and incorporated into the polyurethane scaffold by ultrasonic treatment. Formation of nanoparticles was characterized using Fourier transform infrared, transmission electron microscopy, X-ray photoelectron spectroscopy, and energy dispersive X-ray spectroscopy. Iron oxide nanoparticles (FeONPs) with an average size of 50 nm were not uniformly integrated; however, spherical cerium oxide nanoparticles (CeONPs) with an average size of 14 nm were easily incorporated into the polyurethane scaffold. The CeONP-incorporated polyurethane scaffold was highly responsive (<10 s) to $H_2O_2$, with a limit of detection of 3.18 μM, and was reusable for at least ten cycles without significant loss of detection activity. However, the response time of CeONP solution was more than 5 min. Both FeONP solution and FeONP incorporated polyurethane scaffold were poor at detecting $H_2O_2$.

Keywords: Cerium Oxide Nanoparticles, Iron Oxide Nanoparticles, Polyurethane Scaffold, Hydrogen Peroxide Detection, Reusability

## INTRODUCTION

Hydrogen peroxide ($H_2O_2$) plays a key role in the regulation of many physiological processes, and has seen wide applications in the food processing industry, paper bleaching process, and in antiseptic/disinfecting agents [1-3]. $H_2O_2$ has been utilized therapeutically for wound irrigation and sterilization of ophthalmic and endoscopic instruments. However, excessive $H_2O_2$ (>35%) use can cause cell mutation [4], which further leads to many severe diseases including cancer, neurodegeneration, Parkinson's and Alzheimer's diseases [5]. In addition, high concentration of $H_2O_2$ generates free radicals that can cause high oxidative stress in the cells. Corrosive damage and lipid peroxidation are also caused by high concentration of $H_2O_2$. Therefore, major researches have focused on developing and improving numerous techniques to detect minute concentration of $H_2O_2$ in samples. Spectrophotometry, chemiluminescence, fluorescence, and electrochemical methods are some of the most common and popular analytical techniques that have been developed for quantification of $H_2O_2$ over the last decades [2].

Apart from conventional methods, nanomaterials have attracted much research attention due to their enzyme-like characteristics. Numerous nanomaterials, such as carbon nanotubes, graphene nanosheets [6], gold nanoparticles [7], silver nanoparticles [4], and $Cu_2O$ nanotubes [8], have been explored for the detection of $H_2O_2$ in recent years. These nanoparticles show excellent peroxidase mimic activity, similar to the natural enzyme horseradish peroxidase (HRP) [9]. Conversely, natural enzymes are more prone to small changes in environmental conditions (temperature, pH, salt concentration, etc.) and follow a relatively expensive process for their preparation and purification. Alternatively, nanomaterials are inexpensive, have higher stability, and can provide stable catalytic activities for long periods.

In recent years, cerium and iron oxide nanoparticles have gained diverse attention as catalysts, energy storage devices, optical sensors, and biomedicine due to their robust physical and chemical properties [10]. Cerium has two oxidation states ($Ce^{3+}$ and $Ce^{4+}$), and its reversible switching of catalytic performance depends on the ratio of these states [11]. Peroxidase and catalase mimic activities are prominent at higher $Ce^{4+}/Ce^{3+}$ ratios, whereas superoxide dismutase mimic activity becomes more persistent at lower ratios [11]. Moreover, the ratio of these two oxidation states typically depends on the synthesis process and microenvironmental conditions. Several conventional chemical synthesis methods, such as sonochemical, hydrothermal, and ball milling solvothermal, have been adopted for the synthesis of cerium oxide nanoparticles (CeONPs) [11]. However, the use of toxic solvents, harsh operating conditions (high temperature and pressure), and environmental hazards caused by these chemicals are some of the major limitations of this process. As the properties of CeONPs strongly depend on their oxidation states, greater attention should be paid to controlled synthesis.

Likewise, iron oxide nanoparticles (FeONPs) have also demonstrated attractive prospects in the field of biochemical applications such as protein immobilization and separation, cancer hypothermia, and drug delivery [1,3,12,13]. Recently, magnetic nanoparticles (MNPs) have drawn research attention as an alternative to natural enzymes due to their low cost and high stability. MNPs are very well known for their peroxidase and catalase mimic activities [13-16].

†To whom correspondence should be addressed.
E-mail: bskim@chungbuk.ac.kr
Copyright by The Korean Institute of Chemical Engineers.

Among several MNPs, $Fe_3O_4$ and $Fe_2O_3$ nanoparticles are extremely popular for their intrinsic peroxidase activity, which is essentially due to the ferrous ions residing on the surface of the nanoparticles. This mechanism follows the Fenton reaction, which includes the formation of OH radicals from the reaction of $Fe^{2+}$ and $H_2O_2$. Subsequently, these OH radicals oxidize 3,3′,5,5′-tetramethylbenzidine (TMB) to produce a blue color that can be quantified by spectroscopy. As the uncoated $Fe_2O_3$ nanoparticles lack peroxidase activity, various coatings have been used to enhance the activity. Recent studies have reported the use of Prussian blue and porphyrin to modify the surfaces of nanoparticles for enhanced activity [15-17]. It has been well demonstrated that FeONPs exhibit better peroxidase activity under acidic condition, unlike the natural enzyme HRP, which favors neutral pH [1,18,19]. Extensive studies have been carried out on chemically synthesized FeONPs and their peroxidase mimic activity.

The major limitations of nanoparticles are often associated with their agglomeration in solution due to high surface energy and their lack of reusability, both of which hinder the overall performance [3]. In addition, in the overall sensing process, nanoparticles tend to settle very quickly and become unstable. Furthermore, solution-based peroxide detection assays are prone to small traces of contaminants and often create environmental hazards on disposal. Therefore, immobilization of nanoparticles over suitable support [2,3,20,21] should provide a major alternative in terms of higher stability and reusability for multiple cycles [20]. Immobilization also increases the shelf-life of nanoparticles and decreases the overall process cost. In the present study, a novel approach was developed using immobilized cerium and iron oxide nanoparticles for the detection of $H_2O_2$. These nanoparticles were immobilized over bio-based polyurethane scaffold, which was prepared using soybean oil and malic acid. The synthesized and immobilized nanoparticles were characterized using a variety of techniques and were adapted as an alternative to the natural enzyme HRP. To the best of our knowledge, this is the first report on the rapid and stable detection of $H_2O_2$ using reusable polymer nanocomposites.

## MATERIALS AND METHODS

### 1. Materials

Soybean oil (average 4.6 double bonds per molecule), 1,6-hexamethylene diisocyanate (HMDI), dibutyltin dilaurate (DBTDL), and 3,3′,5,5′-tetramethylbenzidine (TMB, >99.0%) were purchased from Sigma-Aldrich. Sodium acetate was supplied from Sigma Life Sciences. Cerium nitrate hexahydrate ($Ce(NO_3)_3{\cdot}6H_2O$, 99.0%), acetic acid ($CH_3COOH$, >99%), hydrogen peroxide ($H_2O_2$, 34.5%), sodium chloride (NaCl, 99.0%), ether (99%), acetone (99.5%), and polyethylene glycol (PEG, $M_n$: 4000) were procured from Samchun Chemicals (Korea). Sulfuric acid (95%) and ammonia solution (28%) were purchased from OCI Company Ltd. (Korea). DL-malic acid (MA) was purchased from Tokyo Chemical Industry Co. Ltd. (Japan). Iron (III) chloride hexahydrate ($FeCl_3{\cdot}6H_2O$, 99.0%), iron (II) chloride tetrahydrate ($FeCl_2{\cdot}4H_2O$, 97.0%), and tetrahydrofuran (THF) were purchased from Junsei Chemical Co. Ltd. (Japan). All chemicals were used as received without any further modification, unless mentioned. All standard solutions were prepared using double distilled water.

### 2. Synthesis of Epoxidized Soybean Oil-Malic Acid (ESO-MA) Polyol and ESO-MA Polyurethane (ESO-MA PU) Scaffold

Polyurethane was prepared as reported in our previous study [22]. Briefly, 50 g of soybean oil was epoxidized at 60 °C for 4 h in presence of 3 wt% $H_2SO_4$ as a catalyst. Subsequently, the synthesized ESO and malic acid were mixed at a molar ratio of 1 : 2 for 12 h at 60 °C. The synthesized ESO-MA polyol was washed three times with an ample amount of water and dried over $Na_2SO_4$. Dried ESO-MA polyol (2 g) was mixed with 1% w/v of DBTDL for 5 min at room temperature, followed by addition of HMDI at an NCO/OH molar ratio of 1.4 and further mixing for 5 min. The polymer reaction mixture had 4 g NaCl and 1 mL distilled water added to it, followed by vigorous stirring for 10 min. After completion of the process, the polymer mixture was cast over a polytetrafluoroethylene coated glass plate, followed by drying under vacuum at 50 °C for 5-8 min to degas $CO_2$. Air was injected to avoid sample deformation under vacuum and subsequently the sample was cured at 80 °C for 18 h. The resulting polyurethane scaffold was washed for 12 h to eliminate excess NaCl, followed by drying at 80 °C.

### 3. Synthesis of CeONPs

CeONPs were synthesized by the method described previously [23]. PEG 4000 (10% w/v in $H_2O$) was added to 0.2 M of cerium nitrate hexahydrate under continuous stirring for 1 h. Final pH of the mixture was adjusted to 3 by 0.1 N nitric acid. Stoichiometric amount of $H_2O_2$ was added dropwise to the mixture, which was mixed thoroughly until the color turned from colorless to orange. Subsequently, the final mixture was centrifuged at 15,000 rpm for 30 min, followed by three times washing with water and ethanol. Finally, the recovered nanoparticles were freeze-dried and stored for further use.

### 4. Synthesis of FeONPs

FeONPs were synthesized as reported previously [24] with slight modification. Ammonia was added at 1 : 1 (v/v) ratio to distilled water along with 1 M $FeCl_2$ and 2 M $FeCl_3$, followed by stirring at 60 °C overnight. The formed nanoparticles were washed with distilled water, followed by freeze drying.

### 5. Synthesis of CeONP and FeONP-incorporated ESO-MA PU Scaffold

CeONP was incorporated in the polyurethane scaffold by dip-coating method using ultrasound. 0.5 mg/mL CeONPs were dispersed in distilled water using a probe sonicator (125 W, 20 KHz) for 15-20 min [25]. ESO-MA polyurethane scaffold was dipped into the prepared dispersion under mild sonication (820 W, 60 Hz) for 2 h, followed by overnight drying. Polyurethane scaffold incorporating nanoparticles was washed with an ample amount of water to remove excess nanoparticles, and subsequently dried in an oven at 80 °C. A similar method was followed for the incorporation of FeONPs in the polyurethane scaffold.

### 6. Detection of $H_2O_2$ Using CeONP Solution and CeONP-incorporated PU Scaffold

Reaction mixture containing 330 μL acetate buffer (0.2 M, pH 4.16), 300 μL TMB (6 mM), 100 μL $H_2O_2$, and 50 μL CeONP (0.5 mg/mL) was added to a 24 well plate, mixed for 30 s and incubated for 30 min at room temperature. Subsequently, the absorbance of the mixture was recorded at 652 nm and 450 nm before and after

addition of 1 N $H_2SO_4$, respectively. For the detection of $H_2O_2$ using the scaffold, a similar procedure was followed, while replacing CeONP solution with 10 mg of CeONP-incorporated scaffold. In both studies, the concentration of $H_2O_2$ in the mixture was changed from 500 nM to 200 μM.

**7. Detection of $H_2O_2$ using FeONP Solution and FeONP-incorporated Scaffold**

A method similar to that described in the previous section was followed for the detection of $H_2O_2$ using FeONPs and the FeONP-incorporated scaffold. However, prior to detection, the freeze-dried FeONPs were subjected to ultrasonication in distilled water for 2 h.

**8. Reusability of CeONP-incorporated ESO-MA PU Scaffold**

Reusability study of CeONP-incorporated ESO-MA PU scaffold was carried out for ten consecutive cycles. After completion of one cycle (i.e., the detection process), the scaffold was washed with ethanol and immersed in the same for 30 min, followed by drying at 80 °C for 15 min to evaporate the solvent. The same method was followed for next cycles. The relative activity was calculated using Eq. (1).

$$\text{Relative activity}\,(\%) = \frac{n^{th}\ \text{absorbance}}{\text{Initial absorbance}} \times 100 \quad (1)$$

**9. Analytical Methods**

Fourier transform infrared (FTIR) analysis was conducted using a Nicolet Magna-IR 200 FTIR spectrometer (Thermo Fisher Scientific, Waltham, MA, USA). ESO and ESO-MA samples were mixed with KBr to form pellets prior to analysis. ESO-MA PU, CeONP, FeONP, CeONP-PU, and FeONP-PU samples were thin-filmed by mixing with KBr to make pellets with a final sample/KBr ratio of 1 : 100. The spectra were collected in a range of 4,000-400 $cm^{-1}$ with a spectral resolution of 32 $cm^{-1}$ and 64 scans. Size of nanoparticles was determined by transmission electron microscopy (TEM). One drop of CeONP and FeONP suspension was dried on a carbon coated copper grid, which was finally analyzed using TEM (Carl Zeiss, Libra 120), operated at 120 kV. Surface morphologies of CeONP-PU scaffold and FeONP-PU scaffold were investigated using scanning electron microscopy (SEM, Carl Zeiss, LEO-1530, 20 kV). Small amounts of nanoparticles and a scaffold were placed over the stub, air dried, and platinum coated prior to analysis. Elemental analyses of nanoparticles and nanoparticle-incorporated scaffolds were performed using an energy dispersive X-ray spectroscopy (EDS, Thermo Fisher Scientific, Resolution 128 eV). Prior to the analysis, samples were placed on a template, air dried, and platinum coated. The oxidation states of the synthesized nanoparticles were investigated by X-ray photoelectron spectroscopy (XPS, PHI Quantera-II, 20 kV) with an Al K$\alpha$=1,486.6 eV excitation source. The absorbance of nanoparticle suspension and scaffold for detection of $H_2O_2$ was investigated using an X-mark microplate spectrophotometer (Bio-Rad Laboratories). This study was carried out using a 24 well microplate with sample volume ranging from 500 to 3,000 μL.

## RESULTS AND DISCUSSION

**1. Synthesis of ESO-MA Polyol and ESO-MA PU Scaffold**

Characterization of synthesized ESO-MA polyol and ESO-MA PU using FTIR, NMR, and mass spectroscopy analysis was discussed in our previous study [22]. After ESO-MA polyol synthesis, the ESO-MA based PU was prepared with an NCO/OH ratio of 1.4 and characterized further by FTIR (Fig. S1). Shifting of the broad peak (representing the -OH group) from 3,470 $cm^{-1}$ to 3,390 $cm^{-1}$ in the ESO-MA PU spectrum represents the formation of N-H stretching in the PU structure [26,27]. The bands at 1,537 $cm^{-1}$ and 1,730 $cm^{-1}$ correspond to N-H bending and the C=O group, respectively [28,29]. In addition, amide carbonyl stretching and C-O-C bond are confirmed at peaks of 1,650 $cm^{-1}$ and 1,100 $cm^{-1}$, respectively. Absence of a peak at 2,270 $cm^{-1}$ confirms no presence of HMDI in the mixture, which further verifies the reaction of all the HMDI molecules with polyol.

**2. Characterization of Synthesized Nanoparticles**

FTIR spectra of cerium nitrate hexahydrate ($Ce(NO_3)_3{\cdot}6H_2O$) and CeONPs are depicted in Fig. 1(a). The $Ce(NO_3)_3{\cdot}6H_2O$ spectrum exhibited stretching and bending at 3,400 and 1,600 $cm^{-1}$, respectively, representing attachment of water molecules. Also, the bands at 1,450 and 1,350 $cm^{-1}$ correspond to nitrate ion vibrations. The formation of a Ce-O group can be verified from the transmittance peak at 610 $cm^{-1}$ in the spectra. The characteristic peak at 1,064 $cm^{-1}$ corresponding to -OH and C-O-H stretching confirms the presence of PEG in the structure. In addition, a new peak at 2,920 $cm^{-1}$ indicating -$CH_2$ band also corroborates the presence of PEG coating on the nanoparticles. The TEM image of CeONPs (Fig. 1(b)) shows that the nanoparticles are not monodisperse and agglomeration persisted [10,30]. The obtained nanoparticles were spherical with an average size of ~14 nm. Elemental compositions of synthesized nanoparticles were studied using EDS spectra (Fig. 1(c)). The peak at 4.839 keV indicates the presence of cerium in the dried nanoparticles. In addition, the presence of carbon and oxygen peaks in the spectra indicates the amorphous nature of the polymer coating [31]. The presence of carbon and oxygen hinders precise estimation of the cerium to oxygen ratio from the EDS spectrum. The surface oxidation state of CeONP was further investigated using XPS analysis (Fig. 1(d) and 1(e)). The presence of a signal at ~284.5 eV represents the C1s peak, which further testifies to the successful conjugation of PEG with the nanoparticles [23]. The peaks at 897.9 and 916.23 eV correspond to Ce (IV) $3d^9 4f^0 O^{2p6}$, whereas peaks at 882.18 and 901.10 eV are attributed to Ce (IV) $3d^9 4f^2 O^{2p4}$ [23,32]. However, the peaks at 886.18 and 904.3 eV can be assigned to Ce (III) $3d^9 4f^2 O^{2p5}$, which indicates the formation of mixed valences in the nanoparticles [32]. Nonetheless, the peaks representing $Ce^{4+}$ are much stronger than those representing $Ce^{3+}$, which can be attributed to the higher ratio of $Ce^{4+}/Ce^{3+}$. The O1s spectra can be well fitted at ~531 and 528 eV; this is attributed to the binding energies of the oxygen atoms bonded to the hydroxyl groups [23].

FTIR spectrum of FeONPs is shown in Fig. S2. The peaks at 3,440 $cm^{-1}$, 2,927 $cm^{-1}$, and 1,754 $cm^{-1}$ can be attributed to -OH stretching, -CH stretching, and -C=O groups, respectively. The characteristic peak at 586 $cm^{-1}$ represents the formation of Fe-O in the nanoparticle structure. The absorption band at 1,632 $cm^{-1}$ can be attributed to the presence of carbonyl stretching. The band at 1,400 $cm^{-1}$ represents -OH bending vibrations. The synthesized FeONPs were spherical with an average size of 50 nm [24]. The EDS spec-

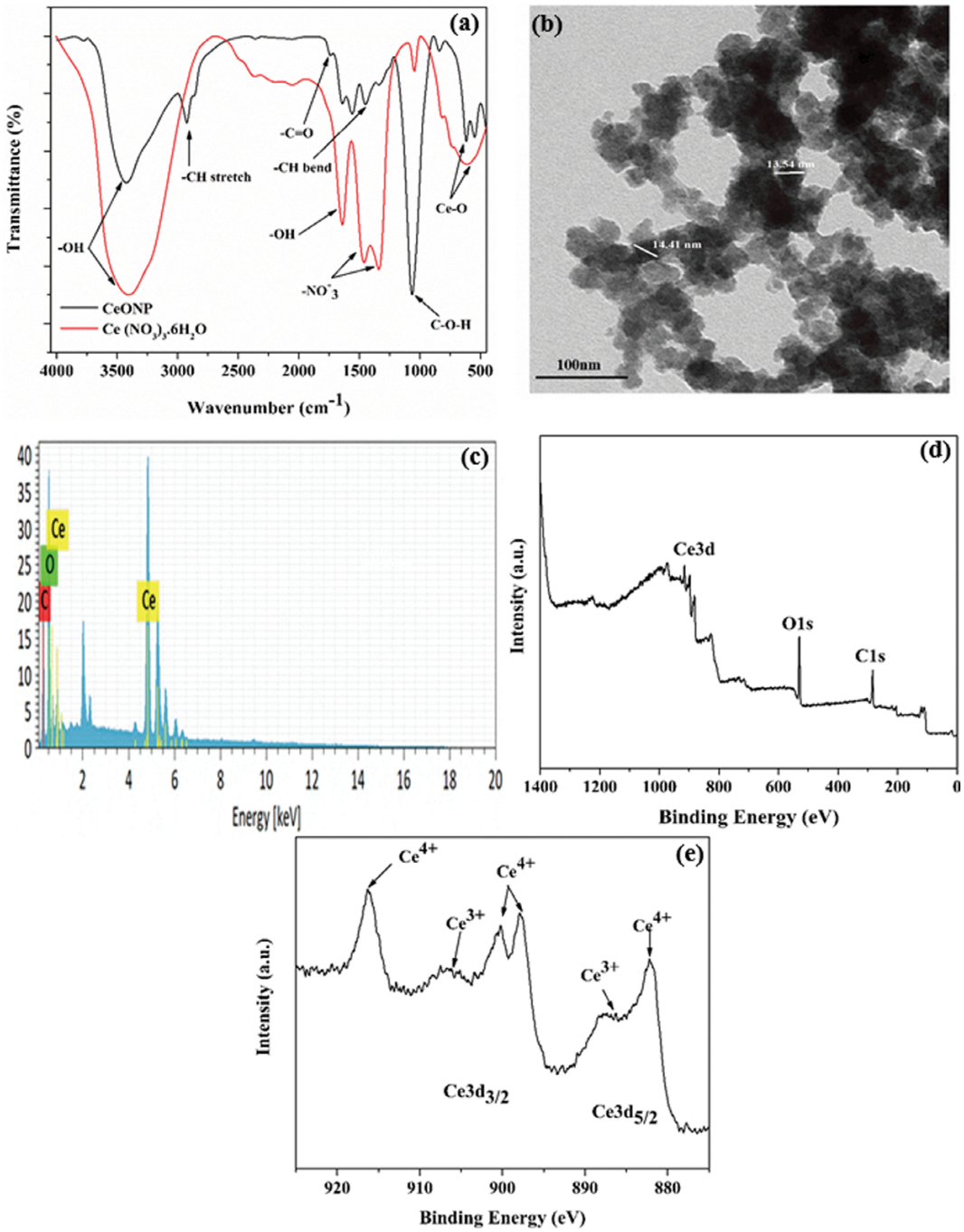
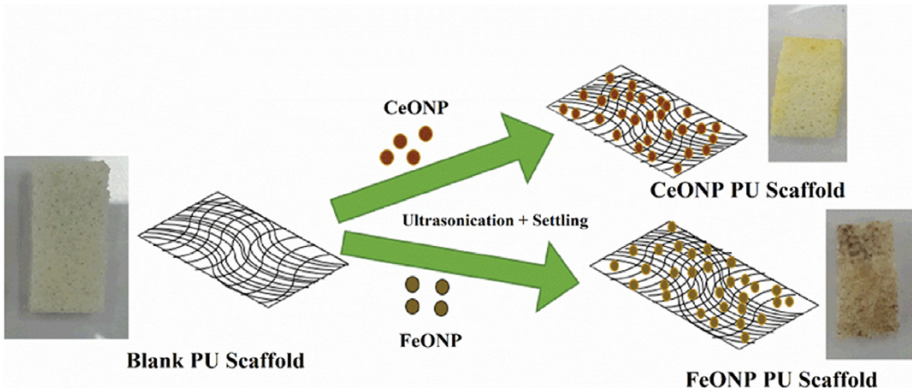



**Fig. 1. (a) FTIR spectra of $Ce(NO_3)_3 \cdot 6H_2O$ and PEG-coated CeONPs. (b) TEM images of CeONPs. (c) EDS spectra of CeONPs. (d) XPS spectra of CeONPs. (e) $Ce3d_{3/2,5/2}$ XPS spectra collected for CeONPs.**

trum in Fig. S3 of chemically synthesized FeONPs reveals the presence of iron peaks in three different areas at 0.7, 6.4, and 7.2 keV. The formation of FeONPs can be confirmed by the presence of oxygen peaks in the spectrum. From the spectrum, the atomic ratio of iron to oxygen was found to be 3 : 4.

### 3. Characterization of Synthesized Nanoparticle Incorporated PU Scaffold

Ultrasonic treatment is effective for deposition and insertion of nanoparticles into the polymer scaffold [24]. Incorporation of CeONP in the polyurethane scaffold was confirmed by a change in color of the scaffold from white to yellow (Scheme 1). The color change in the scaffold was evenly distributed on its surface, which confirms the uniformity of the nanoparticles on the surface and the effectiveness of the ultrasonic treatment. Further analysis confirmed the incorporation of ~2.5 wt% of nanoparticles into the scaffold by this technique. FTIR spectrum of polyurethane scaffold confirms the incorporation of CeONPs in the ESO-MA polyurethane matrix (Fig. S1). The presence of Ce-O groups inside the




**Scheme 1. Schematic diagram illustrating the synthesis of nanoparticle incorporated PU scaffold.**

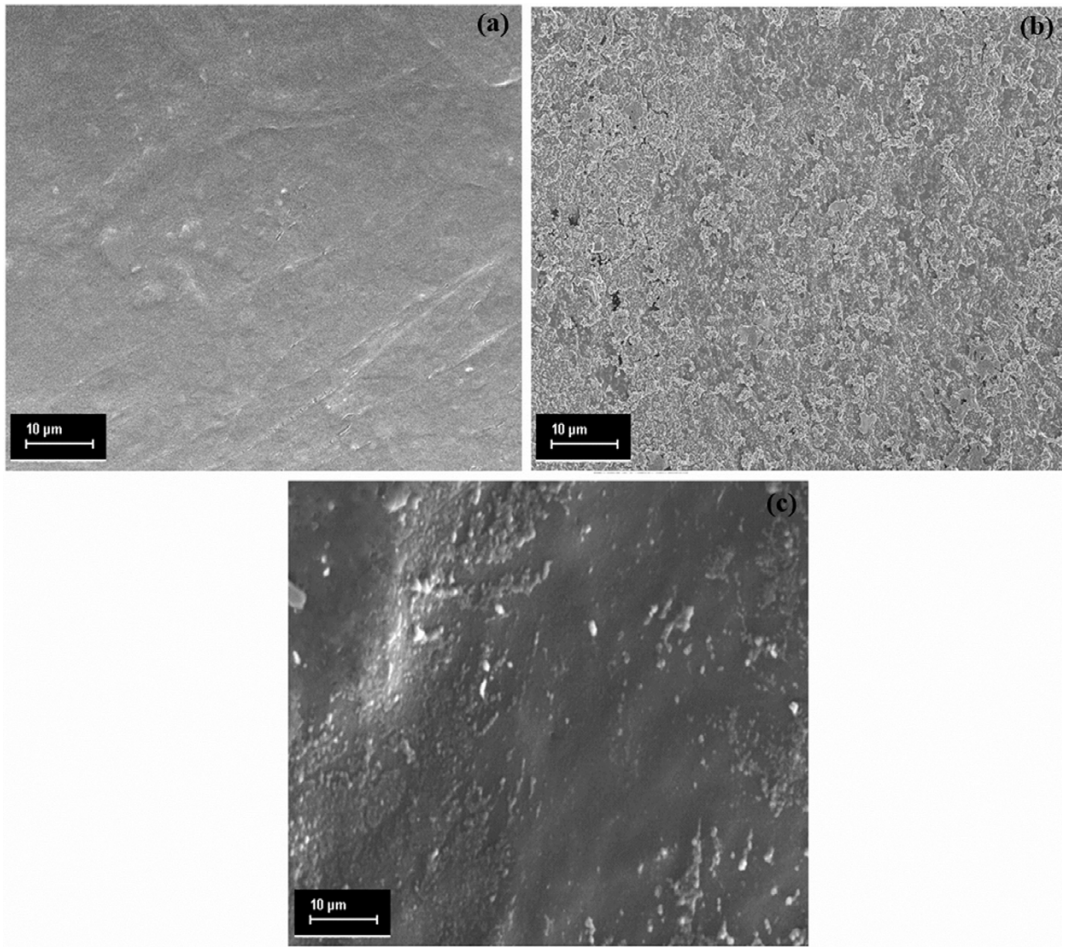



**Fig. 2. FESEM spectra of (a) ESO-MA PU scaffold, (b) CeONP ESO-MA PU scaffold, and (c) FeONP ESO-MA PU scaffold.**

polymer structure is associated with the peak at 610 $cm^{-1}$, as compared to the spectrum of blank ESO-MA PU (Fig. S1).

FeONPs were inserted into the surface pores of the polymer by ultrasonication, and this was further substantiated by a change in color of the polymer surface from white to brown as shown in Scheme 1. However, due to the rapid agglomeration of nanoparticles, uniform distribution of nanoparticles over the polymer could not be achieved. This resulted in uneven distribution of color over the surface of the FeONP-incorporated scaffold. A new peak at 650 $cm^{-1}$ in the FTIR spectrum (Fig. S1) indicates the presence of Fe-O in the polyurethane structure, as compared to ESO-MA PU [16]. SEM data (Fig. 2) show that incorporation of nanoparticles increased the roughness of the scaffold surface. EDS data also supported successful incorporation of nanoparticles into the scaffold surface (Fig. 3). CeONPs (Fig. 3(b)) were found to be more efficiently incorporated into PU (~19%) than FeONPs (~0.18%) (Fig.

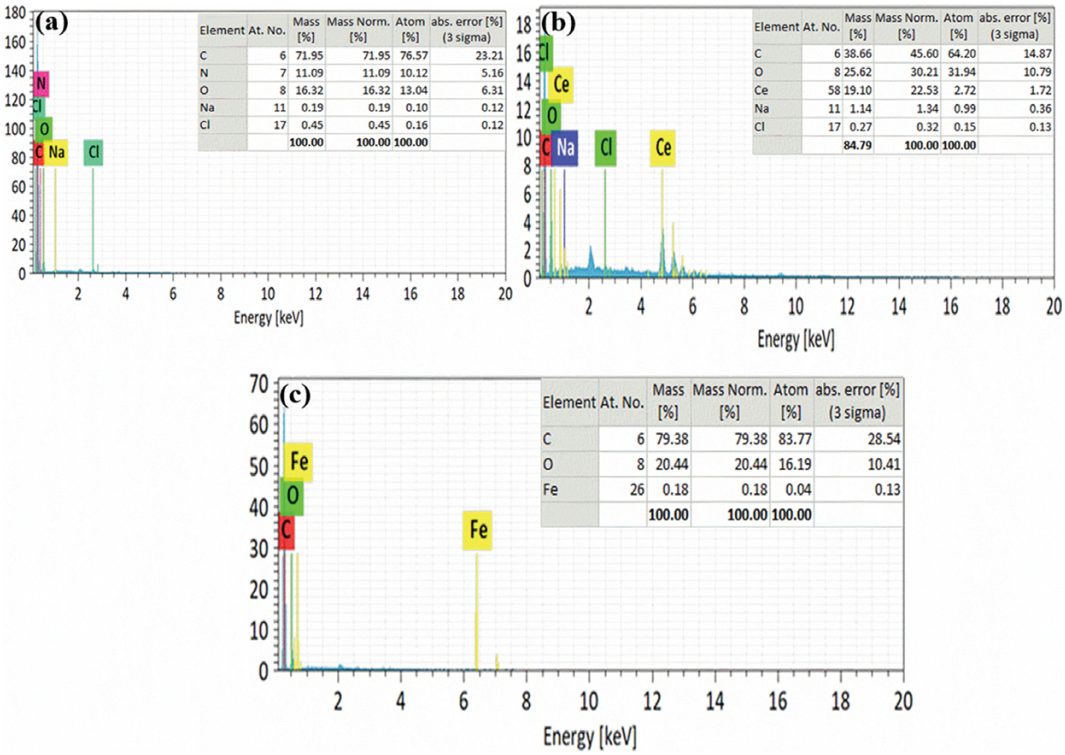



**Fig. 3. EDS spectra of (a) ESO-MA PU scaffold, (b) CeONP ESO-MA PU scaffold, and (c) FeONP ESO-MA PU scaffold.**

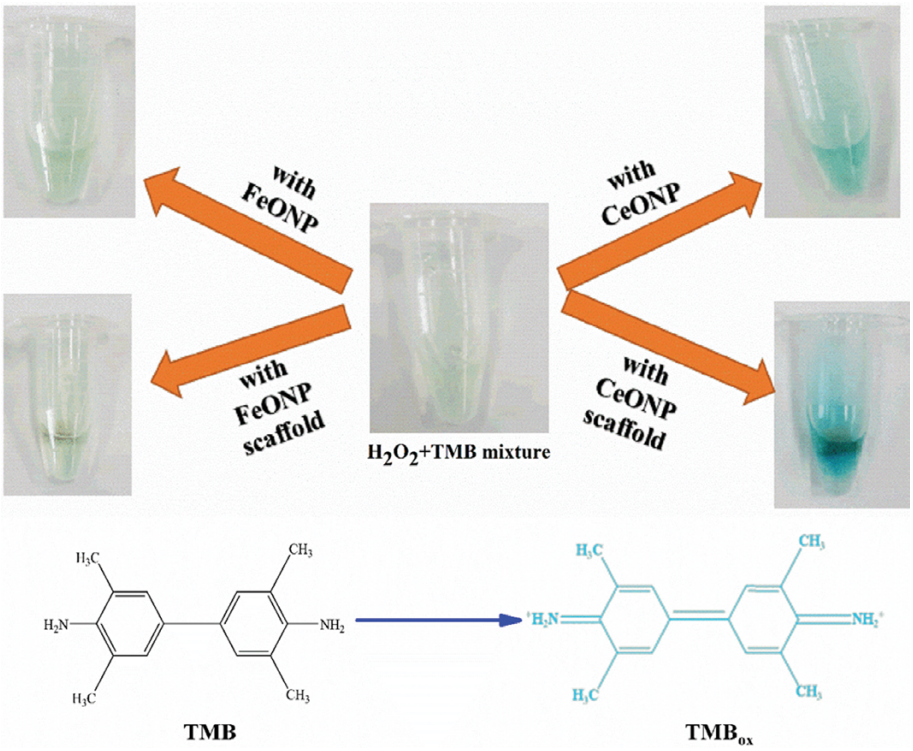



**Fig. 4. Comparison of detection ability between CeONP, FeONP, and their corresponding scaffolds.**

3(c)). This phenomenon could be corroborated by the high magnetic property of the nanoparticles [14], which causes faster agglomeration and difficult dispersion in the solution. Furthermore, the obtained FeONPs were bigger than CeONP. These properties of nanoparticles prevented their effective insertion into the surface of the PU scaffold.

**4. Investigation of CeONP and FeONP for Colorimetric Detection of $H_2O_2$**

For the detection of $H_2O_2$, TMB was chosen as a chromogenic substrate that can be effectively oxidized by $H_2O_2$ in the presence of nanoparticles as a catalyst to form a blue imine product ($TMB_{ox}$) (Fig. 4). Without CeONP, $H_2O_2$ failed to oxidize TMB at room temperature and change its color (Fig. 4). In contrast to the peroxidase activity of other nanoparticles, PEG-coated CeONPs have the ability to oxidize TMB in absence of $H_2O_2$, where it serves as an electron acceptor [23]. The presence of oxidized TMB in the mixture was indicated by an absorbance peak at 652 nm (UV images are not shown). Optimal activity of CeONPs was observed at pH 4.0 and 55 °C [11]. However, the produced CeONPs were able to detect micromolecular concentration of $H_2O_2$ at room temperature (25 °C), and a decrease in absorbance value was noticed with an increase in peroxidase concentration (Fig. S4(a)). A plausible explanation for this could be the dissociation of $H_2O_2$ (at micromolar concentration) to hydroperoxy or perhydroxy radicals in acidic condition (pH 4.16) (Eq. (2)). This radical further converted $Ce^{4+}$ to $Ce^{3+}$, with associated oxidation of TMB to $TMB_{ox}$ (Eq. (3)) [33-35].

$$H_2O_2 = HO_2^{\bullet} + H^+ + e^- \quad (2)$$

$$Ce^{4+} + HO_2^{\bullet} = Ce^{3+} + H^+ + O_2 \quad (3)$$

Therefore, an increase in peroxide concentration increased the $Ce^{3+}/Ce^{4+}$ ratio on the surface of the nanoparticles, which further led to inhibition of the oxidase mimic activity [11,23,34]. In addition, the lower pH interfered with the autocatalytic nature of the CeONPs due to high concentration of protons, and hence inhibited the oxidase mimic activity [32]. Another possible reason is that $H_2O_2$ molecules at its low concentration adsorbed on the nanoparticle surface preventing the contact between TMB and CeONP [23]. The reaction was terminated with the addition of 1 N $H_2SO_4$, which changed the color of the reaction mixture to orange, giving an absorbance maximum at 450 nm (UV images are not shown) [23]. $H_2SO_4$ changed the pH of the mixture abruptly, which led to the deactivation of catalytic activity of CeONPs. It was also noticed that the absorbance value dropped significantly with the increase in $H_2O_2$ concentration. Therefore, the inhibition of oxidase activity of CeONP by $H_2O_2$ can be used as an indicator for the development of a highly sensitive $H_2O_2$ detection system. An empirical linear relationship was established (Fig. 5(a)) between the absorbance ratio at 652 nm and 450 nm, i.e., A652/A450, with peroxide concentration in the range of 8-100 μM and a limit of detection (LOD=3S/b where S is the standard deviation of blank samples and b is slope of the linear plot) of 1.72 μM [23]. The obtained LOD is lower than those of the dextran-coated cerium oxide nanoparticles [23], synthesized $Cu_2(OH)_3Cl$-$CeO_2$ nanocomposite [36], and porphyrin functionalized nanoceria [37], but higher than those of HRP immobilized nanoceria film [38] and nanostructured C/$CeO_2$

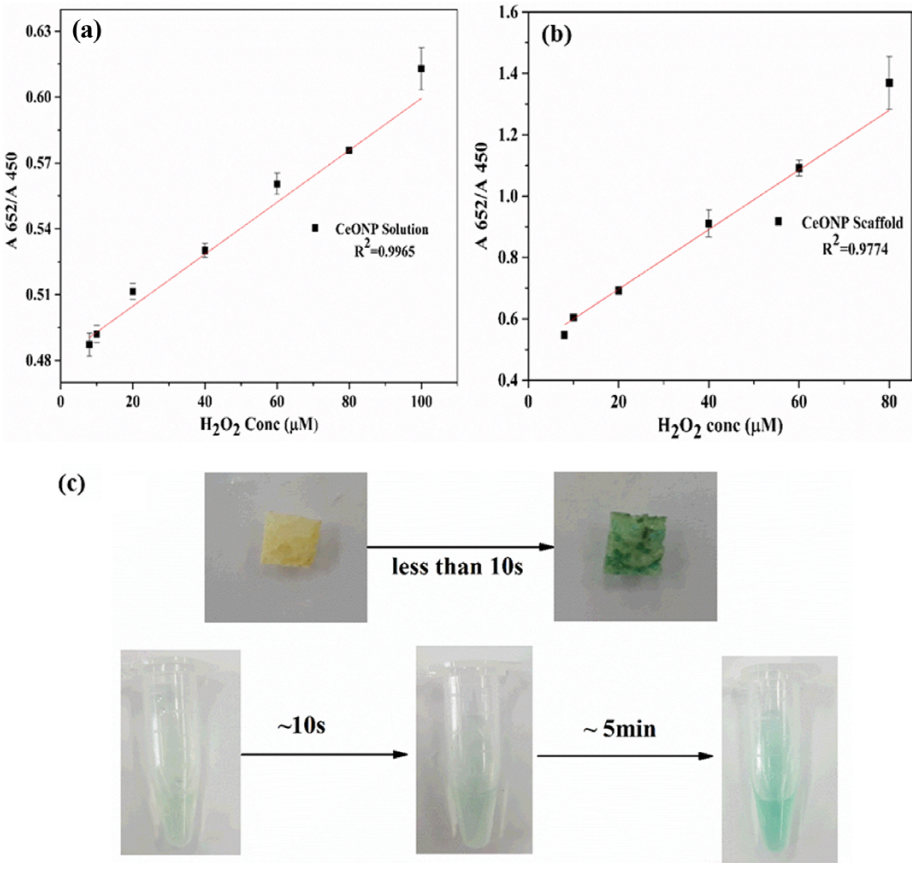



**Fig. 5. Linear detection curve (a) for CeONP solution and (b) for CeONP ESO-MA PU scaffold. (c) Comparison of response between CeONP solution and CeONP ESO-MA PU scaffold.**

**Table 1. Summary of $H_2O_2$ detection using various solution-based and membrane/scaffold-based sensors**

| Sensor | Limit of detection of $H_2O_2$ (LOD) | Response time | Reusability | Reference |
|---|---|---|---|---|
| Solution-based | | | | |
| Dextran-coated CeONP | 2 μM | - | - | [23] |
| $Cu_2(OH)_3Cl$-$CeO_2$ nanocomposite | 10 μM | - | - | [36] |
| Porphyrin functionalized CeONP | 6.1 μM | - | - | [37] |
| PEG-coated CeONP | 1.72 μM | 5 min | - | This work |
| Membrane/Scaffold-based | | | | |
| Gold nanoparticle polysulfone nanofibrous membrane | 0.5 μM | <10 sec | - | [2] |
| Gold nanoparticle-incorporated agar membrane | 20 μM | - | - | [3] |
| Silver nanoparticle-sputtered nanofibrous membrane | 4 μM | - | - | [41] |
| HRP immobilized chitosan gelation nanofiber biocomposite | 50 μM | - | - | [42] |
| PEG-coated CeONP ESO-MA PU scaffold | 3.18 μM | <10 sec | Up to 10 cycles | This work |

hollow framework [9]. The correlation coefficient ($R^2$) was 0.9965.

On the other hand, a weak detection ability was noticed for FeONPs at room temperature in an acidic environment (Fig. 4). Lower absorbance values and less intense color change were obtained for FeONPs than for CeONPs (Fig. S4(a)). According to the previous study, iron oxide nanoparticles show optimal peroxidase mimic activity at 37-40 °C and pH 4.0 (acetate buffer) [14,16,17]. Although the pH of the acetate buffer was the same as that obtained by other previously described methods, the reaction was performed at room temperature (25 °C), which might affect the dissociation of $H_2O_2$. Here, both concentrations of FeONP (0.5 mg/mL) and $H_2O_2$ (0.5-200 μM) were lower than reported previously [14,15]. In addition, bare iron oxide nanoparticles did not show any peroxidase activity due to lack of ferrous ion over the surface of the nanoparticles [16,39]. Previous studies reported that coating of nanoparticles with carbon nitride nanotubes [40], porphyrin [16], Prussian blue modified $\gamma$-$Fe_2O_3$, and amine group template coated $Fe_2O_3$ nanoparticles [39] led to higher peroxidase mimic activity. The presence of iron in the structure of porphyrin and Prussian blue contributed to the enhanced peroxidase activity.

**5. Study of CeONP and FeONP-incorporated ESO-MA Polyurethane Scaffold for Detection of $H_2O_2$**

The desorption characteristic of the nanoparticles from the surface of the polymer scaffold was investigated by stirring the scaffold in distilled water for 24 h at room temperature. It was estimated that ~0.5% w/w nanoparticles are lost from the surface of polyurethane. Moreover, the non-biodegradable nature of nanoparticles contributed to their stability inside the polymer matrix.

A trend similar to that of the CeONPs was observed in the CeONP-incorporated scaffold (Fig. S4(b)), followed by a linear relationship between A652/A450 and $H_2O_2$ concentration (Fig. 5(b)). It was observed that the LOD for the CeONP incorporated scaffold was 3.18 μM, which was higher than that of the nanoparticle solution. However, it was lower than those of the gold nanoparticle-incorporated membrane (20 μM) [3], silver coated polyacrylonitrile nanofiber membrane (4 μM) [41], and HRP immobilized electrospun chitosan gelation nanofibers (50 μM) [42]. The synthesized CeONPs were mostly inserted into the pores present on the polymer scaffold surface, which ultimately led to low detection range of hydrogen peroxide at room temperature. As shown in Fig. 5(c), the addition of scaffold to mixture solution immediately changed its color from light yellow to bluish green in <10 s. However, color change from yellow to bluish green occurred after 5 min when using nanoparticle solution. The larger surface area of the polyurethane scaffold enhanced the interaction between CeONP and the analytes, which contributed to the rapid sensing performance of $H_2O_2$ [2]. Table 1 summarizes $H_2O_2$ detection ability of various solution-based and membrane/scaffold-based sensors. Compared to the previous reports, this study shows a rapid and reusable detection of $H_2O_2$ with similar or lower LOD.

On the other hand, the FeONP-incorporated polyurethane scaffold showed very weak detection ability towards $H_2O_2$, as shown in Fig. 4. The obtained absorbance values were much lower than those from the CeONP PU scaffold (Fig. S4(b)). As shown in EDS spectra (Fig. 3(c)), FeONPs were not easily inserted inside the pores of the scaffold, which further led to low detection ability. Due to the superior detection ability towards $H_2O_2$, the CeONP PU scaffold was further selected for reusability study.

**6. Reusability of CeONP-incorporated ESO-MA PU Scaffold**

A reusability study of the CeONP solution was not feasible due to the low concentration of nanoparticles in the mixture. This also led to difficulty in separation from the resultant mixture and loss of CeONPs during washing. On the other hand, the produced CeONP polyurethane scaffold was easy to reuse and could be used for multiple cycles without any significant loss of its activity (Fig. 6). The reusability of the scaffold was studied at $H_2O_2$ concentration 200 μM. Fig. 6(a) shows the sequential colorimetric responses of the scaffold up to 10 cycles. It was observed that washing the scaffold with ethanol and 30 min immersion in same was able to bring back the original color for at least ten cycles and the relative activity (determined from Eq. (1)) did not decrease significantly (Fig. 6(b)) (>75% after ten cycles). Similar results were observed in the previous study with Whatman filter paper [20]. The color change of the scaffold occurred due to its interaction with the chromogenic substrate TMB and its high solubility in ethanol. The TMB associated with the scaffold surface can be easily washed away and thus the scaffold can regain its original color. Therefore, a scaffold can be helpful in preventing loss of nanoparticle solution and reduce

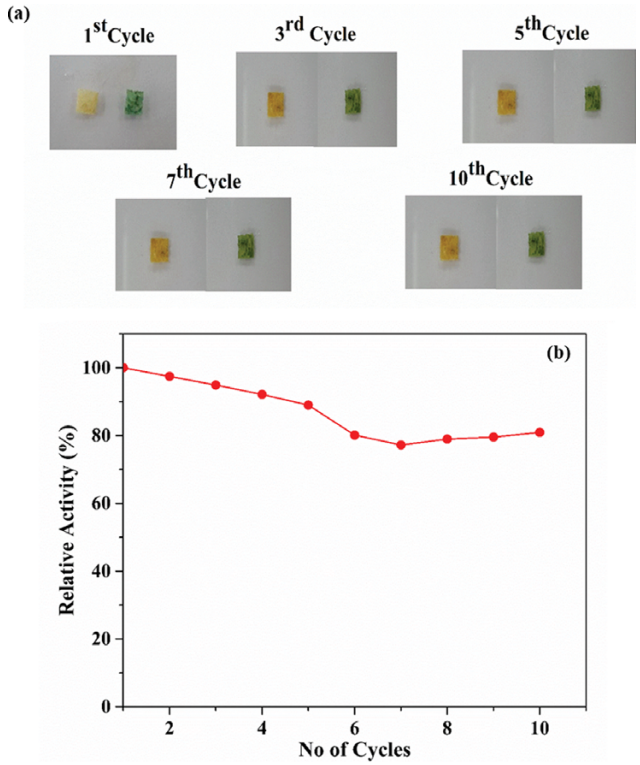



**Fig. 6. Reusability of assay after washing CeONP-PU scaffold with ethanol: (a) Pictures showing colorimetric responses after 1, 3, 5, 7, and 10 cycles. (b) Relative activity of scaffold in multiple cycles.**

the overall cost of the process.

## CONCLUSION

The peroxidase mimic abilities of both cerium and iron oxide nanoparticles were compared for solution and scaffold phases. The synthesized nanoparticles were incorporated by ultrasound treatment into the surface of the ESO-MA PU scaffold. The response rate of the scaffold for the detection of $H_2O_2$ was much faster than that of the solution phase. In addition, the CeONP-incorporated scaffold had a lower LOD than those of previously reported membranes and was reusable for multiple cycles without significant loss of activity. CeONPs in both solution and membrane phases showed higher peroxidase mimic activity and detection ability towards $H_2O_2$ than the FeONPs. This stable nanoparticle-incorporated scaffold can be useful in optical sensing, fluorescent imaging, and photovoltaics, as well as *in vivo* applications.

## ACKNOWLEDGEMENT

This research was supported by the National Research Foundation of Korea (NRF-2017R1A2B4002371 and 2019R1I1A3A02058523).

## SUPPORTING INFORMATION

Additional information as noted in the text. This information is available via the Internet at http://www.springer.com/chemistry/journal/11814.

## REFERENCES

1. W. Chen, S. Cai, Q. Q. Ren, W. Wen and Y. D. Zhao, *Analyst*, **137**, 49 (2012).
2. A. Senthamizhan, B. Balusamy, Z. Aytac and T. Uyar, *Anal. Bioanal. Chem.*, **408**, 1357 (2016).
3. P. Zhang, Y. Wang and Y. Yin, *Sensors*, **16**, 1124 (2016).
4. A. N. Naik, S. Patra, A. S. Kanekar, D. Sen, S. V. Ramagiri, J. R. Bellare, S. Mazumder and A. Goswami, *Sensor. Actuat. B. Chem.*, **255**, 605 (2018).
5. B. C. Dickinson, Y. Tang, Z. Chang and C. J. Chang, *Chem. Biol.*, **18**, 943 (2011).
6. D. Cai and M. Song, *J. Mater. Chem.*, **20**, 7906 (2010).
7. Y. J. Long, Y. F. Li, Y. Liu, J. J. Zheng, J. Tang and C. Z. Huang, *Chem. Comm.*, **47**, 11939 (2011).
8. M. Liu, R. Liu and W. Chen, *Biosens. Bioelectron.*, **45**, 206 (2013).
9. N. Wang, J. Duan, W. Shi, X. Zhai, F. Guan, L. Yang and B. Hou, *Microchim. Acta*, **185**, 417 (2018).
10. F. Caputo, M. Mameli, A. Sienkiewicz, S. Licoccia, F. Stellacci, L. Ghibelli and E. Traversa, *Sci. Rep.*, **7**, 4636 (2017).
11. F. Charbgoo, M. Ramezani and M. Darroudi, *Biosens. Bioelectron.*, **96**, 33 (2017).
12. R. Khodadust, G. Unsoy, S. Yalcın, G. Gunduz and U. Gunduz, *J. Nanopart. Res.*, **15**, 1488 (2013).
13. M. Aghazadeh, I. Karimzadeh, M. G. Maragheh and M. R. Ganjal, *Korean J. Chem. Eng.*, **35**, 1341 (2018).
14. L. Gao, K. Fan and X. Yan, *Theranostics*, **7**, 3207 (2017).
15. H. Wei and E. Wang, *Anal. Chem.*, **80**, 2250 (2008).
16. Q. Liu, L. Zhang, H. Li, Q. Jia, Y. Jiang, Y. Yang and R. Zhu, *Mater. Sci. Eng. C.*, **55**, 193 (2015).
17. S. Zhang, X. Zhao, H. Niu, Y. Shi, Y. Cai and G. Jiang, *J. Hazard. Mater.*, **167**, 560 (2009).
18. A. Mishra, R. Ahmad, M. Perwez and M. Sardar, *BioNanoScience*, **6**, 93 (2016).
19. F. Yu, Y. Huang, A. J. Cole and V. C. Yang, *Biomaterials*, **30**, 4716 (2009).
20. M. Ornatska, E. Sharpe, D. Andreescu and S. Andreescu, *Anal. Chem.*, **83**, 4273 (2011).
21. D. Kumar and N. Talreja, *Korean J. Chem. Eng.*, **36**, 126 (2018).
22. P. Saha and B. S. Kim, *J. Polym. Environ.*, **27**, 2001 (2019).
23. R. Guo, Y. Wang, S. Yu, W. Zhu, F. Zheng, W. Liu, D. Zhang and J. Wang, *RSC Adv.*, **6**, 59939 (2016).
24. J. Y. Song, E. Y. Kwon and B. S. Kim, *Korean J. Chem. Eng.*, **29**, 1771 (2012).
25. M. K. Poddar, K. Vishwakarma and V. S. Moholkar, *Korean J. Chem. Eng.*, **36**, 828 (2019).
26. Y. Li and X. S. Sun, *J. Am. Oil Chem. Soc.*, **91**, 1425 (2014).
27. S. Miao, S. Zhang, Z. Su and P. Wang, *J. Polym. Sci. Pol. Chem.*, **48**, 243 (2010).
28. Z. Li, R. Zhang, K. S. Moon, Y. Liu, K. Hansen, T. Le and C. P. Wong, *Adv. Funct. Mater.*, **23**, 1459 (2013).
29. S. S. Narine, X. Kong, L. Bouzidi and P. Sporns, *J. Am. Oil Chem. Soc.*, **84**, 55 (2007).

30. B. Choudhury, P. Chetri and A. Choudhury, *J. Exp. Nanosci.*, **10**, 103 (2015).
31. M. Breitwieser, C. Klose, A. Hartmann, A. Büchler, M. Klingele, S. Vierrath, R. Zengerle and S. Thiele, *Adv. Energy Mater.*, **7**, 1602100 (2017).
32. J. M. Perez, A. Asati, S. Nath and C. Kaittanis, *Small*, **4**, 552 (2008).
33. V. Baldim, F. Bedioui, N. Mignet, I. Margaill and J. F. Berret, *Nanoscale*, **10**, 6971 (2018).
34. D. Dutta, R. Mukherjee, M. Patra, M. Banik, R. Dasgupta, M. Mukherjee and T. Basu, *Colloid. Surf. B*, **147**, 45 (2016).
35. H. Cheng, S. Lin, F. Muhammad, Y. W. Lin and H. Wei, *ACS Sensors*, **11**, 1336 (2016).
36. N. Wang, J. Sun, L. Chen, H. Fan and S. Ai, *Microchim. Acta*, **182**, 1733 (2015).
37. Q. Liu, Y. Ding, Y. Yang, L. Zhang, L. Sun, P. Chen and C. Gao, *Mater. Sci. Eng. C.*, **59**, 445 (2016).
38. A. A. Ansari, P. R. Solanki and B. D. Malhotra, *J. Biotechnol.*, **142**, 179 (2009).
39. A. Roy, R. Sahoo, C. Ray, S. Dutta and T. Pal, *RSC Adv.*, **6**, 32308 (2016).
40. J. W. Lee, H. J. Jeon, H. J. Shin and J. K. Kang, *Chem. Comm.*, **48**, 422 (2012).
41. D. Li, L. Luo, Z. Pang, X. Chen, Y. Cai and Q. Wei, *RSC Adv.*, **4**, 3857 (2014).
42. S. Teepoo, P. Dawan and N. Barnthip, *Biosensors*, **7**, 47 (2017).

# Supporting Information

# Rapid and reusable detection of hydrogen peroxide using polyurethane scaffold incorporated with cerium oxide nanoparticles

**Pathikrit Saha, Anoth Maharajan, Pritam Kumar Dikshit, and Beom Soo Kim†**

Department of Chemical Engineering, Chungbuk National University, Cheongju, Chungbuk 28644, Korea
(*Received 8 August 2019 • accepted 1 October 2019*)

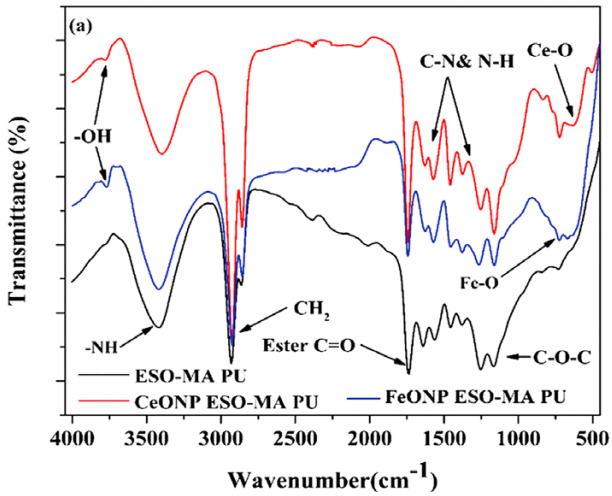



**Fig. S1. FTIR spectra of ESO-MA PU, CeONP ESO-MA PU and FeONP ESO-MA PU.**

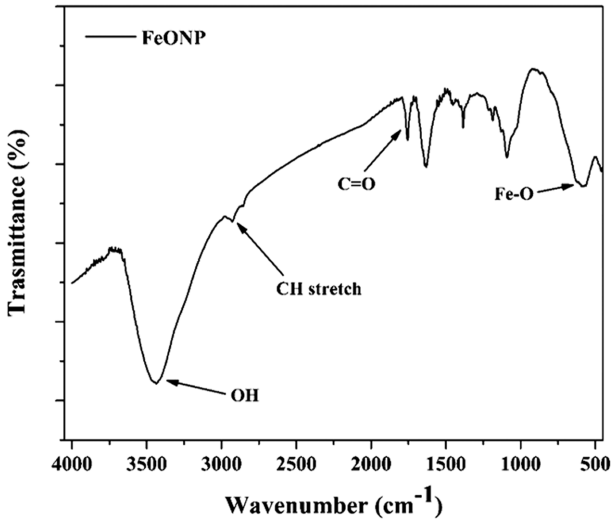



**Fig. S2. FTIR spectra of FeONP.**

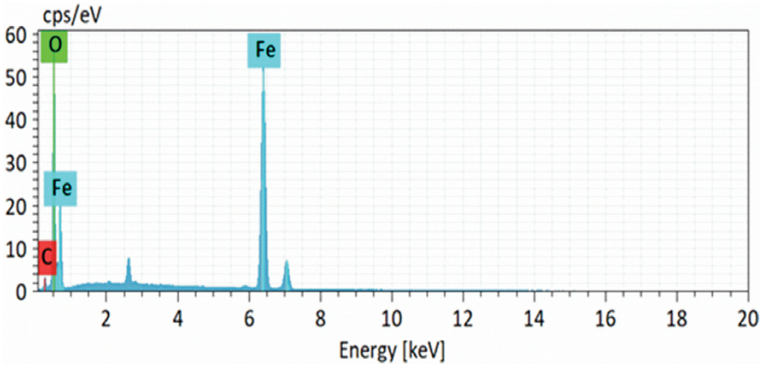



**Fig. S3. EDS spectra of FeONP.**

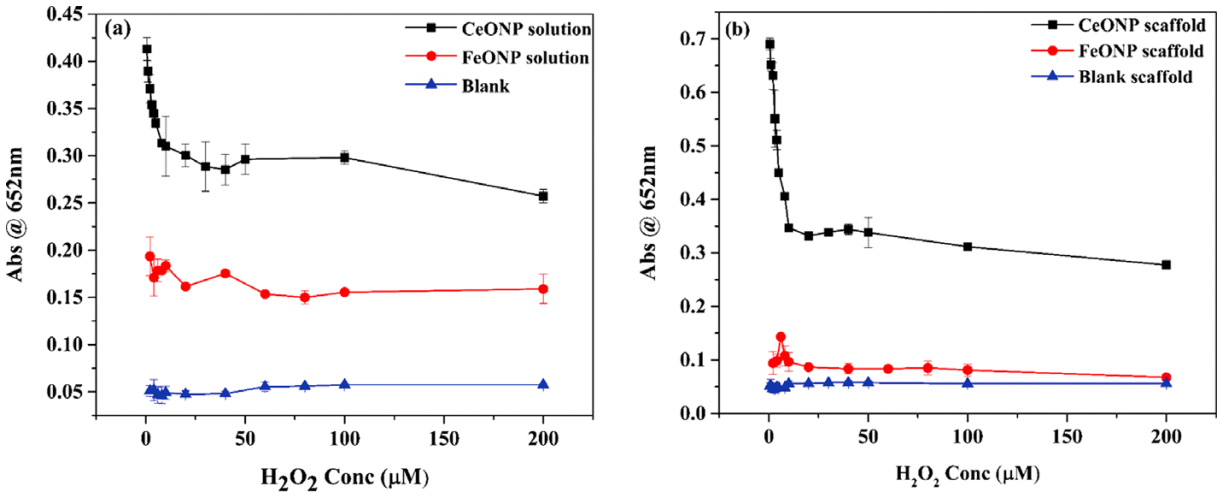



**Fig. S4. (a) Effect of $H_2O_2$ concentration on absorbance for nanoparticle solution. (b) Effect of $H_2O_2$ concentration on absorbance for PU scaffold.**